Check for updates

Optics Letters

High coupling efficiency waveguide grating couplers on lithium niobate

Xuetong Zhou,[1] Ying Xue,[2] Fan Ye,[1] Ziyao Feng,[1] Yuan Li,[1] Xiankai Sun,[1] Kei May Lau,[1,2] and Hon Ki Tsang[1,*]

[1] Department of Electronic Engineering, The Chinese University of Hong Kong, Shatin, Hong Kong, China
[2] Department of Electronic and Computer Engineering, Hong Kong University of Science and Technology, Kowloon, Hong Kong, China
*hktsang@ee.cuhk.edu.hk

Received 10 March 2023; revised 28 April 2023; accepted 16 May 2023; posted 16 May 2023; published 12 June 2023

We propose and validate a new, to the best of our knowledge, approach for high coupling efficiency (CE) grating couplers (GCs) in the lithium niobate on insulator photonic integration platform. Enhanced CE is achieved by increasing the grating strength using a high refractive index polysilicon layer on the GC. Due to the high refractive index of the polysilicon layer, the light in the lithium niobate waveguide is pulled up to the grating region. The optical cavity formed in the vertical direction enhances the CE of the waveguide GC. With this novel structure, simulations predicted the CE to be −1.40 dB, while the experimentally measured CE was −2.20 dB with a 3-dB bandwidth of 81 nm from 1592 nm to 1673 nm. The high CE GC is achieved without using bottom metal reflectors or requiring the etching of the lithium niobate material. © 2023 Optica Publishing Group

https://doi.org/10.1364/OL.489753

Lithium niobate on insulator (LNOI) has attracted much interest in recent years because it combines the well-known advantages of lithium niobate (LN) for photonics [1] in a high-index contrast platform suitable for making extremely compact and high-speed modulators. LNOI wafers are readily available commercially based on the smart-cut technique and wafer-bonding process [2,3]. One of the challenges in improving the performance of the LNOI platform is the development of a manufacturable high yield, relaxed alignment tolerance and low-loss interface between the LNOI waveguide and optical fiber. Waveguide grating couplers (GCs) are an attractive approach for the fiber–chip photonic interface because of their compatibility with wafer scale testing, arbitrary position on the chip, no need for facet polishing, and relaxed alignment tolerance. Unlike the silicon photonics platform, where waveguide GCs can be manufactured with fiber-waveguide coupling losses of below 1 dB without the use of substrate mirrors [4], it is much more challenging to realize high coupling efficiency (CE) GCs without substrate mirrors on the LNOI platform. Previous works on the development of GCs for the LNOI platform were able to achieve a 1.43 dB [5] and 0.89 dB [6] coupling loss only with the use of additional metal mirror in the substrate to improve the directionality of the GC. A GC with a coupling loss of 3.06 dB using hybrid amorphous silicon on an etched LN platform without metal mirror has also been reported [7]. Dry etching of LN to produce vertical sidewalls is difficult to control and may adversely impact the yield. Hence, to avoid this difficulty, silicon on lithium niobate has been previously proposed to make GCs for the LNOI platform. However, the CE reported was only −18 dB [8]. Silicon nitride on LN has also been proposed for a GC, but the coupling efficiencies reported were only −4.02 dB [9] and −5.82 dB [10].

In this paper, we propose and experimentally validate a novel approach which can attain high CE in the LNOI platform without the need for etching of LN nor the fabrication of substrate mirrors. The experimental demonstration of the concept was implemented on the bound states in the continuum (BIC) photonic integration platform on LN [11]. The novelty introduced in this paper is the use of a high refractive index polysilicon overlay layer in combination with an intermediate oxide layer on the LN GC. The silicon oxide layer, being sandwiched between the higher refractive index regions of the polysilicon and LN materials, forms a low refractive index slot waveguide. In this structure, the light originally in the LN layer is pulled up into the grating region, thus increasing the grating strength. The vertical polysilicon-oxide-LN slot structure can also be considered as an optical cavity in the vertical direction. By carefully designing the thicknesses of the deposited silicon oxide and polysilicon layers, we can improve the CE by taking advantage of the enhancement of the optical field stored in the cavity. The 3D finite-difference time-domain (FDTD) simulation results indicate possible coupling losses of as low as 1.40 dB. We fabricated the grating and measured the CE to be −2.20 dB. The designed GC does not need etching of the LN, and with its minimum feature size > 387 nm, the design is robust and suitable for large-volume manufacturing using photolithography, and dry etching of the polysilicon and the oxide layer only. No substrate Bragg reflectors nor metal mirror is required to improve the directionality of the grating, unlike the previously reported high-efficiency GC designs for the LNOI platform [5,6]. The well-established process control for dry etching oxide and polysilicon promises the prospects of high-yield manufacturability of the proposed GC for use in LNOI photonic integrated circuits.

The 2D and 3D schematic diagrams of the proposed GC on LNOI (X-cut) are shown in Fig. 1. Low temperature oxide (LTO) was deposited at 420°C on the 400-nm-thick LN and etched to form the BIC waveguide channels, where careful design of

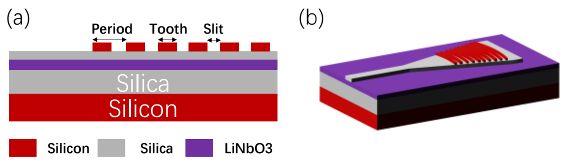

Fig. 1. (a) Schematic of the high CE grating for lithium niobate on insulator. (a) 2D cross section view. (b) 3D view.

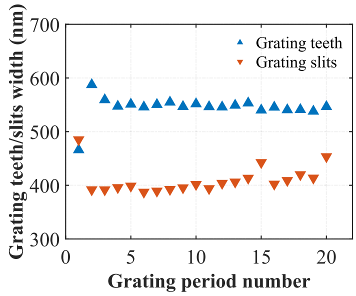

Fig. 2. Final optimized structural parameters for the GC.

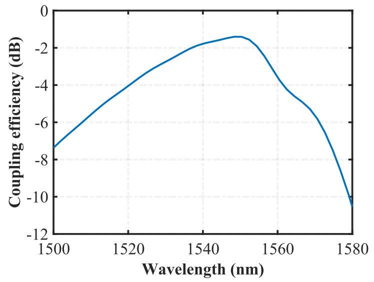

Fig. 3. Simulated CE spectra of the final optimized GC.

the channel widths enabled low loss waveguide propagation as described previously [11]. For the waveguide GCs, low pressure chemical vapor deposition (LPCVD) of the polysilicon layer at 620°C was used. The thicknesses of the LTO and polysilicon layers were carefully engineered to enhance the directionality and the CE (see below). The combined polysilicon overlay with the BIC circuit will form a slot waveguide mode in the vertical direction [12,13], and the light entering the grating region from a BIC waveguide will be pulled up from the high index LN layer, and thus have stronger interaction with the grating. In addition, the high index (polysilicon)–low index (LTO)–high index (LN) structure of the designed grating forms a cavity in the vertical direction. Careful design of the thickness of the LTO and polysilicon can ensure resonance enhancement of the intensity in the cavity and also improve the directionality by having the light scattered upward from the cavity having constructive interference with the light reflected from the underlying dielectric interfaces. The proposed grating may superficially resemble the previously reported GC [7], but the design methodology and working principle are totally different. In Ref. [7], a 90-nm-thick silica layer was simply used as buffer layer between the a-Si and LN thin layer to improve the adhesion of the a-Si, without any design consideration for engineering a vertical cavity or maximizing the directionality. In this paper, we used 300-nm LTO to define the BIC waveguide channel. Furthermore, in Ref. [7], it was still necessary to etch 240 nm of the LN, while for our proposed grating, we do not need any etching of the LN layer. Another key difference is that we used the TM mode in the BIC waveguide (whereas Ref. [7] used the TE mode), and the TM mode has a stronger cavity effect than the TE mode in the vertical direction. The TM mode also has a lower effective index and thus a larger grating period which increases the fabrication tolerance of the GC.

Based on the above design principle, we employed a numerical optimization method, the genetic algorithm [14], to optimize each period of the GC by varying the period and duty cycle of the polysilicon overlay. The optimization algorithm assumed the use of a 400-nm-thick LN on 2-µm-thick buried-oxide layer. We used 2D FDTD simulation to speed up the optimization process. A detailed description of the optimization algorithm can also be found in our previously published paper [15]. Final optimized parameters of each grating period are plotted in Fig. 2. We can see that the minimum feature size is larger than 387 nm, enabling easy fabrication of grating even using photolithography. The final optimized thickness of the LTO and polysilicon layer is 300 nm and 300 nm, respectively. The top polysilicon overlay is fully etched, which simplifies the fabrication process. The proposed GC is designed for standard single-mode fiber with a mode field diameter of 10.4 µm at 1550 nm and couples light from the fiber to the quasi-TM polarization of the BIC waveguide mode. Transmission spectra of the final optimized GC simulated using 3D FDTD is presented in Fig. 3. In the simulation, the ordinary refractive index (n_o) of ~2.21 and an extraordinary refractive index (n_e) of ~2.14 is assumed for the $LiNbO_3$ at 1550 nm. The final optimized GC has a simulated CE of −1.40 dB at 1549 nm with 3-dB bandwidth of 47 nm from 1517 nm to 1564 nm. The grating here was designed for a coupling angle at 5.5 degree off-vertical.

Figure 4 shows the cross sectional view of the |E| profiles for the high GC in the $LiNbO_3$ platform. We can see clearly that when the light enters the grating region, it will be pulled up from the LN layer into the grating region and thus increase the interaction with the grating. The LN BIC photonic circuit has most of the light confined to the LN region and is, therefore, suitable for efficient electrooptic modulation [11,16]. Only in the grating region do we change the light field distribution to pull it up to the grating. For the LN modulator design, to utilize the largest electro-optic coefficient, we should use the TE mode for an X-cut and the TM mode for a Z-cut LN wafer [17]. For the proof of concept demonstration, we used an X-cut LN wafer in this paper, but the design can also be applied to a Z-cut LN wafer. The fabrication tolerance of the proposed BIC-based high-performance GC is also analyzed. We considered possible variations in the thickness of the LTO, thickness of the polysilicon overlay, etched depth in the polysilicon and LTO layer, etched width of the grating groove in the polysilicon layer, and shift error of the polysilicon layer with the LTO layer.

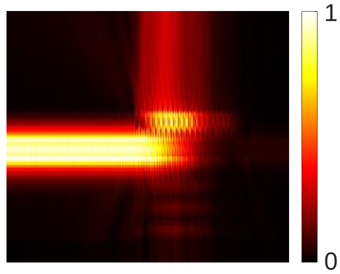

Fig. 4. |E| profiles of the GC working at 1550 nm.

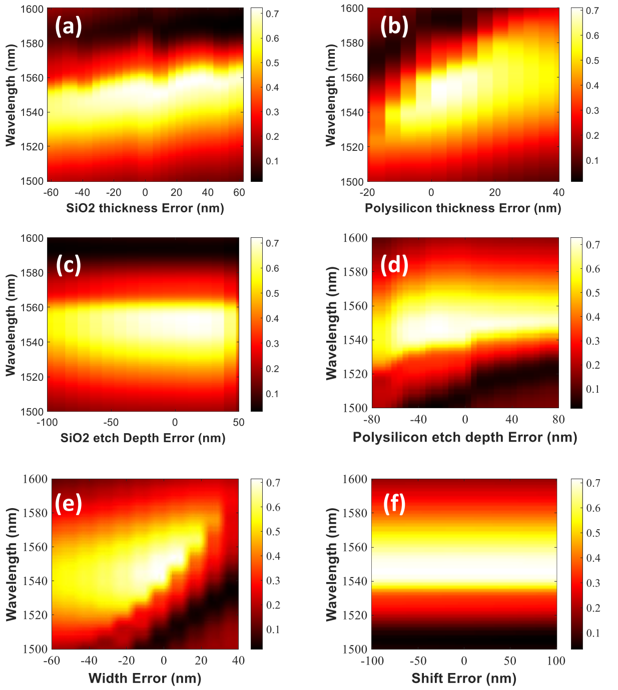

Fig. 5. (a)–(f) CE versus the fabrication variations.

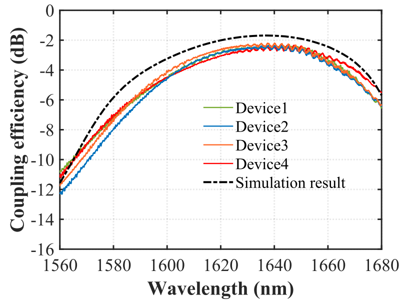

Fig. 6. Experiment results for the grating coupler.

Figures 5(a)–5(f) show the simulated results of the transmission spectra against the parameter fluctuations in the fabrication process. From Figs. 5(a)–5(f), we can see that the CE of the BIC-based high CE GC can withstand a fabrication variation of LTO thickness error variations of +/−60 nm, and polysilicon thickness variations of −20 nm to +40 nm. The high CE is maintained despite LTO etch depth variations of −100 nm to +50 nm and polysilicon layer etch depth variations of −80 nm to +80 nm, etch width of the grating groove variations of −60 nm to +20 nm, and overlay errors between the polysilicon and LTO gratings of +/−100 nm. Furthermore, from the thickness fabrication analysis, we note that the thicker polysilicon layer has better performance over the thinner layers of polysilicon. This is reasonable since increasing the polysilicon overlay will enable more light to be pulled up from the LN region for scattering by the grating.

The CE of the fabricated GC was measured experimentally. In the test devices, we fabricated two focusing BIC-based GCs connected with a straight BIC waveguide. The width of the LTO channel to form the BIC waveguide is 2.3 µm. Measured transmission spectra of a single BIC-based GC is shown in Fig. 6. Several different devices were measured. Waveguide widths for Devices 1 and 2 are 2.3 µm, while for Devices 3 and 4 are 2.1 µm. Device 1 had a peak CE of −2.40 dB per grating at 1643.3 nm with a 3-dB bandwidth of 82 nm from 1592 nm to 1674 nm. Device 2 had a peak CE of −2.35 dB per grating at 1637.8 nm with a 3-dB bandwidth of 79 nm from 1594 nm to 1673 nm. Device 3 had a peak CE of −2.20 dB per grating at 1640.1 nm with a 3-dB bandwidth of 81 nm from 1592 nm to 1673 nm. Device 4 had a CE of −2.32 dB at 1639.9 nm with a 3-dB bandwidth of 86 nm from 1592 nm to 1678 nm.

In the measurement, we assumed negligible propagation losses in the BIC waveguide and identical response of the input and output GCs. Any non-uniformity in the fabrication of the GCs could produce different peak CE wavelengths at input and output, and the performance of individual GC may therefore be better than the averaged measurement result. There is room to further optimize the LPCVD deposition for better thickness and refractive index control of the different layers. In this paper, we used relatively thick LNOI, with a 400-nm-thick LN layer, and it is more difficult to realize high-efficiency GC without etching the waveguide layer. The 400-nm-thick LN here is suitable for efficient electrooptic modulation. By reducing the thickness of the LN layer to 300 nm, better CE may be possible at the cost of lower confinement factor and less efficient modulators. This design method can also be used in realizing high-efficiency GCs for other different thickness LN by changing the thickness of the intermediate LTO and the up polysilicon overlay [13]. The experiment measured center wavelength of the GC was redshifted relative to the simulation predictions. We think this was caused by differences in the parameters (e.g., refractive indices of the different layers and the actual dimensions in the grating structure) of the fabricated device compared with those used in the simulations. Variations of the etched width of the polysilicon groove, etched depth of the LTO layer, and thickness of the LTO and polysilicon may all contribute to the differences between the simulation and experimental results. Another possible source of error in the simulations comes from the use of assumed values for the refractive index of silica and polysilicon that may actually be quite different from the actual values of the LPCVD deposited LTO followed by deposition of polysilicon. Previous studies of LPCVD deposited polysilicon have reported large variations of refractive index from 3.9 to 4.4 at 632.8 nm depending on deposition temperatures [18]. Furthermore, the use of silane gas in the deposition of polysilicon over the LTO layer may result in the introduction of silicon within the LTO layer to form silicon-rich oxide, whose refractive index can vary from 1.48 to 1.99 under different deposited conditions [19]. For example, silicon monoxide (SiO) has a refractive index of 1.877 at 1550 nm, significantly different from the assumed 1.44 index used in the initial simulations. The effect of these possible differences in the refractive indices was studied by further simulations, which showed that when we increase the refractive index of polysilicon from the value used in the initial simulation (3.47 at 1550 nm) to 3.7, and LTO refractive index (initial simulation value was 1.44 at 1550 nm) to 1.87, and we increase the thickness of self-deposited polysilicon by 35 nm and decrease the LTO layer thickness by 9 nm, we obtained the redshift in center wavelength and a better match (the black dotted curve in Fig. 6) with the experiment result. The re-simulation employed the same period and structure parameters of the grating teeth and grating groove as used in the initial simulations. In practice, any etch depth variation of the polysilicon and LTO layer, as well as etch width variations may produce small differences between the

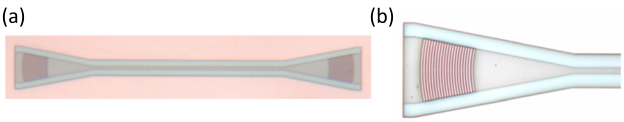

Fig. 7. Microscopy image of the grating coupler. (a) A pair of GCs. (b) Zoom-in of the single grating.

Table 1. Comparison of the Grating Couplers on LNOI

Ref.	LN Etch	Reflector	CE (dB) TE		CE (dB) TM	
			Sim.	Exp.	Sim.	Exp.
[7]	Yes	No	−2.7	−3.06		
[20]	Yes	Yes	−3.13	−3.5	−6.29	−7.12
[21]	Yes	No	−2	−3.6		
[22]	Yes	No	−3	−3.58		
[5]	Yes	Yes	−0.51	−1.43	−1.68	−2.1
[23]	Yes	No	−3	−3.26		
[6]	Yes	Yes	−0.71	−0.89		
[10]	No	No	−4.57	−5.82		
[9]	No	No	−3.21	−4.02		
This work	No	No			−1.40	−2.20

simulations and the experiment results and would account for the experimental variations we observed from Device 1 to Device 4. The experimental results validated the design approach and the simulations point to the importance of precise fabrication process control to achieve consistent results. Even without precise process optimization, we achieved some of the highest coupling efficiencies yet reported for structures without substrate mirrors. We think that with more careful development of the LTO and polysilicon deposition processes, it will be possible to achieve a better CE.

Photograph of the fabricated GC is shown in Fig. 7. We used a focusing grating layout to avoid using long adiabatic tapers between the channel waveguide and the wide grating region needed for matching the mode field diameter of the single-mode fiber. The footprint of the GC was only 55 µm × 24 µm, and the GC is suitable for use in high density photonic integrated circuits. The performance of the GC is compared with previously reported GCs for the LNOI platform in Table 1. The results presented in this paper have the best CE among all the devices that did not require etching of LN. The experimental results are comparable with previous results that required deep etching of LN and the use of bottom metal mirror, and grating apodization with smaller minimum feature sizes [5]. In the BIC photonic circuit, only the oxide needs to be etched, while the GC design presented here also requires a separate etch of the polysilicon layer. The polysilicon grating has a minimum feature size of 387 nm, and is therefore compatible with photolithography. The proposed grating structure is compatible with any LNOI photonic circuits, including those with etched LN waveguides and can be used to develop high modulation speed and high modulation efficiency modulators in the etched LN platform.

To conclude, we proposed and demonstrated a new design of GC that could attain high coupling efficiencies for the LN platform. The proposed design had the advantage of not requiring etching of the LN layer nor the fabrication of substrate mirrors. By forming a vertical cavity structure combined with the BIC circuit enables the grating to attain a high CE. The proposed GC shows good fabrication tolerance and has a minimum feature size above 387 nm, and can be easily fabricated with photolithography. The design was validated experimentally. Measurement results of the fabricated gratings had peak CE of −2.20 dB at 1640.2 nm and a 3-dB bandwidth of 86 nm from 1592 nm to 1678 nm. These results represent some of the highest coupling efficiencies achieved experimentally for TM light using GC in the LNOI platform. It is the best result reported to date for LNOI GCs without using substrate mirrors or etching of the LN layer. The proposed GC will promote the wide use of the emerging $LiNbO_3$ platform and will allow for the utilization of the hybrid advantages of silicon and $LiNbO_3$.

Funding. Research Grants Council (14207021).

Disclosures. The authors declare no conflicts of interest.

Data availability. Data underlying the results presented in this paper are not publicly available at this time.

REFERENCES

1. Y. Qi and Y. Li, Nanophotonics **9**, 1287 (2020).
2. H. Lu, B. Sadani, N. Courjal, G. Ulliac, N. Smith, V. Stenger, M. Collet, F. I. Baida, and M. P. Bernal, Opt. Express **20**, 2974 (2012).
3. G. Poberaj, H. Hu, W. Sohler, and P. Günter, Laser Photonics Rev. **6**, 488 (2012).
4. X. Zhou and H. K. Tsang, IEEE Photonics Technol. Lett. **35**, 43 (2023).
5. S. Kang, R. Zhang, Z. Hao, D. Jia, F. Gao, F. Bo, G. Zhang, and J. Xu, Opt. Lett. **45**, 6651 (2020).
6. B. Chen, Z. Ruan, X. Fan, Z. Wang, J. Liu, C. Li, K. Chen, and L. Liu, APL Photonics **7**, 076103 (2022).
7. J. Jian, P. Xu, H. Chen, M. He, Z. Wu, L. Zhou, L. Liu, C. Yang, and S. Yu, Opt. Express **26**, 29651 (2018).
8. Z. Chen, Y. Wang, H. Zhang, and H. Hu, Opt. Mater. Express **8**, 1253 (2018).
9. X. Han, Y. Jiang, A. Frigg, H. Xiao, P. Zhang, A. Boes, T. G. Nguyen, J. Yang, G. Ren, Y. Su, A. Mitchell, and Y. Tian, APL Photonics **6**, 086108 (2021).
10. Y. Liu, X. Huang, Z. Li, H. Guan, Q. Wei, Z. Fan, W. Han, and Z. Li, Opt. Lett. **45**, 6847 (2020).
11. Z. Yu, X. Xi, J. Ma, H. K. Tsang, C.-L. Zou, and X. Sun, Optica **6**, 1342 (2019).
12. Q. Xu, V. R. Almeida, R. R. Panepucci, and M. Lipson, Opt. Lett. **29**, 1626 (2004).
13. X. Zhou, T. Zhang, L. Chen, W. Hong, and X. Li, J. Lightwave Technol. **32**, 4199 (2014).
14. M. Mitchell, *An Introduction to Genetic Algorithms* (MIT press, 1998).
15. Y. Tong, W. Zhou, and H. K. Tsang, Opt. Lett. **43**, 5709 (2018).
16. Z. Yu and X. Sun, Light: Sci. Appl. **9**, 1 (2020).
17. M. Zhang, C. Wang, P. Kharel, D. Zhu, and M. Lončar, Optica **8**, 652 (2021).
18. T. S. Chao, C. L. Lee, and T. F. Lei, J. Electrochem. Soc. **141**, 2146 (1994).
19. A. Morales-Sánchez, J. Barreto, C. Domínguez-Horna, M. Aceves-Mijares, and J. A. Luna-López, Sens. Actuators, A **142**, 12 (2008).
20. I. Krasnokutska, R. J. Chapman, J. J. Tambasco, and A. Peruzzo, Opt. Express **27**, 17681 (2019).
21. L. Cai and G. Piazza, J. Opt. **21**, 065801 (2019).
22. Z. Ruan, J. Hu, Y. Xue, J. Liu, B. Chen, J. Wang, K. Chen, P. Chen, and L. Liu, Opt. Express **28**, 35615 (2020).
23. E. Lomonte, F. Lenzini, and W. H. P. Pernice, Opt. Express **29**, 20205 (2021).